Powder Technology 293 (2016) 3–14

Contents lists available at ScienceDirect

Powder Technology

journal homepage: www.elsevier.com/locate/powtec

Model tests of silo discharge in a geotechnical centrifuge

J.C. Mathews *, Wei Wu

Institut für Geotechnik, University of Natural Resources and Life Sciences (BOKU), Feistmantelstrasse 4, 1180 Vienna, Austria

ARTICLE INFO

Article history:
Received 9 August 2014
Received in revised form 1 November 2015
Accepted 10 November 2015
Available online 2 December 2015

Keywords:
Silo discharge
Granular material
Model test
Geotechnical centrifuge

ABSTRACT

Scaled models are often used to study the behaviour of silo discharge, however the effects of gravity on silo discharge have not yet been quantified. In this paper, the effects of gravity on silo discharge and internal flow patterns are investigated with reference to the widely used Beverloo correlation. Discharge rate is predicted to be proportional to the square root of gravity and this is demonstrated using experimental results from a novel silo centrifuge model. The effects of changes in gravity on the internal flow profile are also investigated. It is shown that the width of the flow channel at any given height above the outlet is independent of gravity and the local velocity of discharging material is proportional to the square root of gravitational acceleration. These observations show that the angle at which a stagnant zone intercepts a silo wall is independent of gravity and that the criteria for funnel or mass flow conditions are independent of gravity.

1. Introduction

Understanding the effect of stress level on the flow behaviour of material discharging from a silo is important because the stresses experienced in model silos are smaller than those experienced in industrial silos. This makes it difficult to build large silos based on tests of small silos. The strength and flow properties of a bulk granular material are related to the forces between the grains which result from self-weight, normal contact forces and tangential forces, all of which are directly or indirectly proportional to the magnitude of the gravity.

1.1. Silo discharge

In order to predict the rate of silo discharge, Beverloo et al. [1] developed a correlation based on easily measurable silo and material properties. The correlation may be derived using dimensional analysis and calculates the rate of discharge from a silo using material density ρ, gravity g, outlet diameter D and material friction μ.

$$W = f(\rho_b, g, D, \mu) \tag{1}$$

Considering the principles of dimensional analysis and understanding that the coefficient of friction is dimensionless, the only correct form of the relationship between discharge and these variables is

$$W = C\rho_b\sqrt{g}D^{5/2} \tag{2}$$

where C is a coefficient and a function of the coefficient of friction.

Plotting this relationship for a range of orifice diameters in the form $W^{5/2}$ against D shows that the relationship is linear with a non-zero intercept of $W^{5/2}$ on the D axis. Tests with mono-sized particles of different diameters show that the size of the intercept is proportional to particle diameter d and leads to the following correlation:

$$W = C\rho_b\sqrt{g}(D - kd)^{2.5} \tag{3}$$

where C is a coefficient and is almost independent of the particle friction coefficient, ρ_b is bulk density, g is the gravity, D is the orifice diameter, d is the mean particle diameter and k is a coefficient which usually ranges from 1.0–1.5 for spherical particles depending on roughness and is greater for non-spherical particles.

The parameter C is rarely significantly different to 0.58 for a circular orifice. Fowler and Glastonbury [6] suggested a method to calculate a value of C for non-circular outlets based on the assumption that discharge rate is proportional to the product of the outlet area and the square root of the mean hydraulic radius. For a rectangular slot this is $C_{slot} = C_{circ}(4\sqrt{2}/\pi)$, or 1.03. This agrees with work by Myers and Sellers [14] who measured the flow rate of spherical glass beads from wedge hoppers.

The Beverloo correlation may be modified for rectangular outlets by maintaining dimensional consistency and considering that the flow rate increases linearly with silo thickness. The correlation then takes the following form:

$$W = C\rho_b\sqrt{g}(l - kd)(W_0 - kd)^{1.5} \tag{4}$$

where l is the thickness of the silo and W_0 is the width of the outlet. Eq. (4) has been used to predict the flow rate from the model silo, and

* Corresponding author.
E-mail address: jmathews542@gmail.com (J.C. Mathews).

http://dx.doi.org/10.1016/j.powtec.2015.11.025
0032-5910/

the experimental results in Figs. 10 to 12 are compared to discharge rates predicted using this equation.

In addition to the work of Beverloo et al. [1], historical correlations to predict the rate of discharge from a silo include those proposed by Fowler and Glastonbury [6], Ketchum [11], and Ewalt and Buelow [4]. Rose and Tanaka [17] considered the influence of the angle of the stagnant zone and this has been used to modify the Beverloo correlation for a silo which is not flat bottomed. This approach is the same as recommended by the British Materials Handling Board (1987). The only analytical method to calculate discharge rate from a hopper (and not a flat-bottomed silo) is the Hour Glass Theory. It assumes a radial flow field and smooth silo walls which leads to assumed mass flow with no internal shear gradient. This predicts discharge rates that are typically twice as large as observed and is therefore not suitable for application. In industry, the empirical work by Rose and Tanaka[17] is recommended. Rose and Tanaka [17] reported the following correlation:

$$W \propto (\tan\beta\ \tan\phi_d)^{-0.35} \tag{5}$$

when $\beta < 90\text{-}\phi_d$ and where β is the hopper half angle and ϕ_d is the angle between the stagnant zone boundary and the horizontal.

This can be incorporated into the Beverloo equation in the following way:

$$W = W_B F(\beta, \phi_d) \tag{6}$$

where W_B is the discharge rate using the Beverloo correlation and $F(\beta,\phi_d)$ is

$$F(\beta, \phi_d) = (\tan\beta \tan\phi_d)^{-0.35} \qquad \text{for } \beta < 90-\phi_d \tag{7}$$

$$F = 1 \qquad \text{for } \beta > 90-\phi_d. \tag{8}$$

Whilst Beverloo's equation has proven robust and is widely used, few experiments can be found which test its inherent prediction that the discharge rate (W) of cohesionless media from silos is proportional to the square root of acceleration due to gravity ($\sqrt{g}$). Investigations of the influence of gravity on bulk solids include numerical investigations by Chung and Ooi [2] and physical investigations by Dorbolo et al. [3].

1.2. The collapsing arch analogy

The physical origins of the Beverloo correlation can be partially explained by considering a collapsing arch just above the outlet. It has been suggested that the Beverloo correlation exists because there is a free-fall zone above the silo outlet limited by an arch spanning the orifice. Above the arch the particles are well-packed and have very small velocities. Below the arch the particles are in free-fall and accelerate under the action of gravity. If the size of the arch is proportional to the size of the outlet then the velocity of the particles falling through the outlet can be found by calculating the velocity of a particle falling without initial velocity from a distance that is proportional to the width of the outlet.

This analogy encounters problems when considered in more detail. Nedderman [15] argues that the collapsing arch analogy cannot be completely correct because on the surface of the arch the normal stress becomes zero and above the arch the material is subjected to forces resulting from its own mass and also from internal material stresses. Below the arch the material is subjected only to its own body forces. Therefore, as a particle falls through the arch it experiences a reduction in the forces acting on it and its acceleration would reduce. This is incompatible with the acceleration needed to dilate the material and initiate free-fall. Recent work by Rubio-Largo et al. [18] has investigated the collapsing arch analogy and explained its utility despite its physical limitations.

1.3. Flow pattern

The distribution of particle velocities during discharge constitutes a flow pattern, which depends on many factors including granular material properties (particle size distribution and shape), structural factors (wall roughness and hopper angle) and processing history (breakage and segregation). Usually a mass-flow condition is desirable and this is defined as all the material in the silo moving once the outlet is opened (Fig. 1a). However, even when mass flow is produced, it is difficult to ensure that the flow is completely "first in, first out" because this requires that all material above the hopper moves with the same velocity. This is difficult to achieve as the silo walls induce shearing stresses in the material which produces a velocity gradient. The internal shear stresses reduce as distance from the wall increases and thus it is difficult to insure a constant velocity in the cylinder. The alternative to mass flow is funnel flow. This was defined by Jenike [10] as a flow pattern in which some material is stationary while the rest is moving. Different types of funnel flow include parallel pipe flow 1, taper mixed flow 1 and concentric mixed flow 1.

2. Experimental approach

Silo discharge may be better understood by investigating the internal flow response to changes in gravity. This has not yet been widely investigated, perhaps because of the challenges associated with making quantitative observations of internal silo flow during discharge in increased gravity conditions.

In this paper, the velocity of ensiled material during discharge under increased gravity conditions is observed using a planar silo with a transparent front wall through which high speed video of grain displacements is captured. Particle image velocimetry (PIV) is then used to quantify local displacement rates and the results investigated in relation to the body forces exerted. PIV is widely used to measure velocity profiles in one and multiphase flows as shown by Ostendorf and Schwedes [16], Goldschmidt et al. [7], White et al. [20], Gutberlet et al. [8], and Zhuang et al. [21].

2.1. Stress equivalence between scales

Continuum theory predicts that when gravity is increased by the same factor as that by which model geometry is decreased, the same stresses and strains will be produced in the same relative locations in the model as in the prototype. This relationship is utilised in centrifuge modelling techniques which use stress equivalence between scales to model phenomena at reduced scales which are easier to observe. It is demonstrated here using the theory of vertical silo wall pressures presented in Janssen [9], which states that pressures normal to a vertical silo wall may be calculated as follows:

$$q_{\text{prototype}} = \frac{1}{\mu K}\frac{A}{U}\rho_b g\left(1 - e^{-z/\frac{1}{\mu K}\frac{A}{U}}\right) \tag{9}$$

where q is the normal wall pressure, μ is the friction coefficient, K is the lateral pressure ratio, A is the cross sectional area of the silo, U is the wall perimeter, ρ_b is the bulk density, g is the acceleration due to gravity and z is the vertical distance measured from the top of the ensiled material.

If a model-scale silo is built such that the length scale is reduced by a factor of N and gravity is increased by a factor of N then Eq. (9) leads to the following:

$$q_{\text{model}} = \frac{1}{\mu K}\frac{A}{N^2}\frac{N}{U}\rho_b N g\left(1 - e^{-z/\frac{1}{\mu K}\frac{A}{N^2}\frac{N^2}{U}}\right) \tag{10}$$

$$= \frac{1}{\mu K}\frac{A}{U}\rho_b g\left(1 - e^{-z/\frac{1}{\mu K}\frac{A}{U}}\right) = q_{\text{prototype}} \tag{11}$$

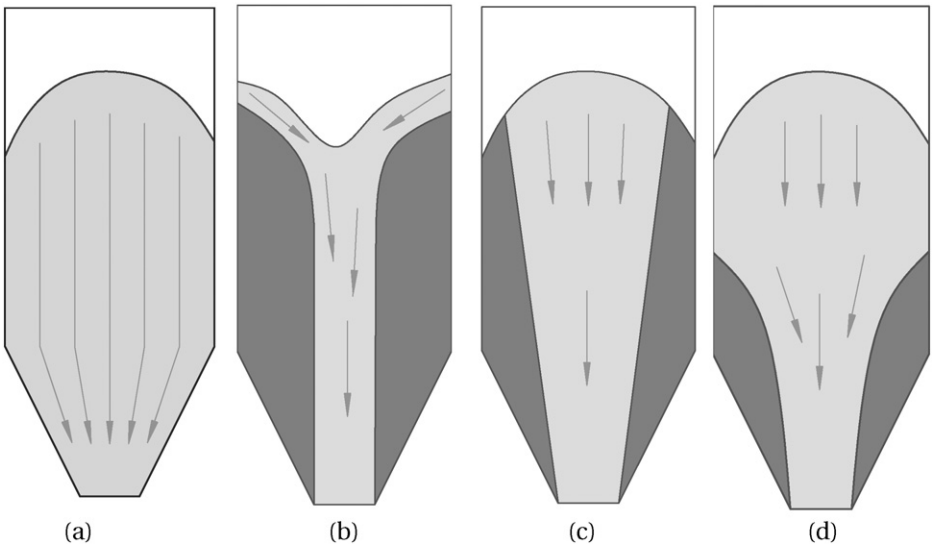

Fig. 1. Types of flow pattern: a) Mass flow. b) Parallel pipe flow. c) Taper mixed flow. d) Concentric mixed flow.

In Eq. (10) the N terms cancel out and the equation becomes the same as Eq. (9). Material properties remain the same at different scales, as they are independent of both the silo geometry and gravity. This shows that equivalent stress states are produced in a prototype and in a model.

A feature of centrifuge modelling is variation of acceleration across the height of a model due to acceleration being proportional to the radius of rotation. Some parts of a centrifuge model are nearer the axis of rotation than others and thus there are small differences in the acceleration experienced at different points. In order to calculate the difference between material stresses produced in a uniform gravitational field and a radially increasing gravitational field, the cumulative effect of the difference between the body forces produced by the two fields is calculated.

Let the model and the prototype both have a free surface where the vertical stress is 0. According to Schofield [19], if R is the target radius of the centrifuge model then there will be a correct pressure p_V in the $1/N$ scale model at radius R. Let the distance between R and the free surface of the model be aR. In the centrifuge model the vertical stress at depth R is found by integrating between the free surface and the target radius. A full description of this treatment can be found in Mathews [13].

In this research, the target radius of the silo centrifuge model corresponds to the distance between the rotational axis and the silo outlet. During flight this is 1.075 m. The distance between the outlet and the top surface of the stored material is approximately 30 cm. The error in the middle of the silo is then calculated using a value of $a = 0.15/1.075$. This gives a difference in vertical stress between the model and the prototype of approximately 3.9%. This small difference is assumed to have a negligible effect on the discharge rate.

3. Experimental set-up

3.1. Description of the IGT beam centrifuge

Silo centrifuge tests took place in the beam centrifuge at the University of Natural Resources and Life Sciences, Vienna. A schematic of the centrifuge design is shown in Fig. 2.

Table 1 lists the centrifuge specifications. A swing basket is hung at each end of the beam and the experimental model is placed into one swing basket and a counterweight is placed into the other. During flight, the motor forces the rotation of the symmetrical aluminium beam. The

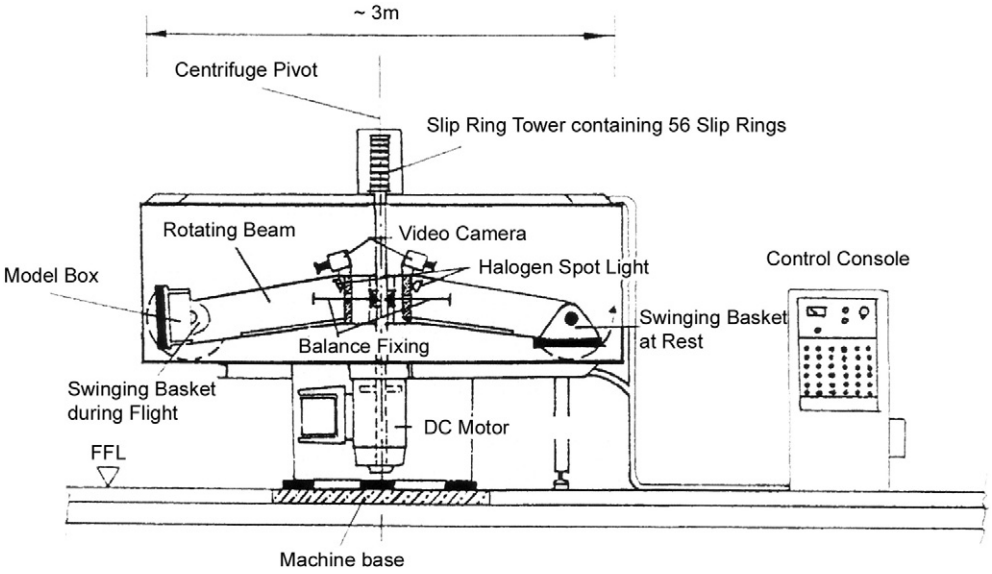

Fig. 2. Schematic sketch of Trio-Tech 1231 Geotechnical Centrifuge, Ferstl. [5].

Table 1
Technical specifications of IGT Beam Centrifuge (TRIO-TECH, 1988).

Property	Value
Diameter of centrifuge [m]	3.0
Radius of swinging basket axis [m]	1.085
Motor	15HP DC
Slip rings	56
Radial acceleration [g]	0 to 200
Rotations per minute [1/min]	0 to 400
Maximum load capacity [G-kg]	10,000
Maximum model mass [kg]	90
Maximum model dimensions W × D × H [mm]	540 × 560 × 560
Total weight [kg]	2041

required centrifugal acceleration is obtained by specifying the rate of angular rotation. After acceleration the velocity is held at a constant level with a stability of ±0.1%.

3.2. Design of the model

The silo centrifuge model (Fig. 3) is designed to behave as a quasi-two-dimensional silo and has dimensions 15 cm×10 cm×29 cm (width, depth, height). It can be configured as either a flat-bottomed silo or with a 30° hopper. It is filled at 1 *g* whilst the centrifuge is stationary using a custom designed funnel. The funnel has a central rectangular outlet 8 mm wide and 10 cm deep. It creates a symmetrical (quasi-two-dimensional) heap of material in the silo during filling. Technical drawings showing the design of the model silo can be found in Mathews [13]. The silo outlet width can be set continuously between 0 mm and 30 mm.

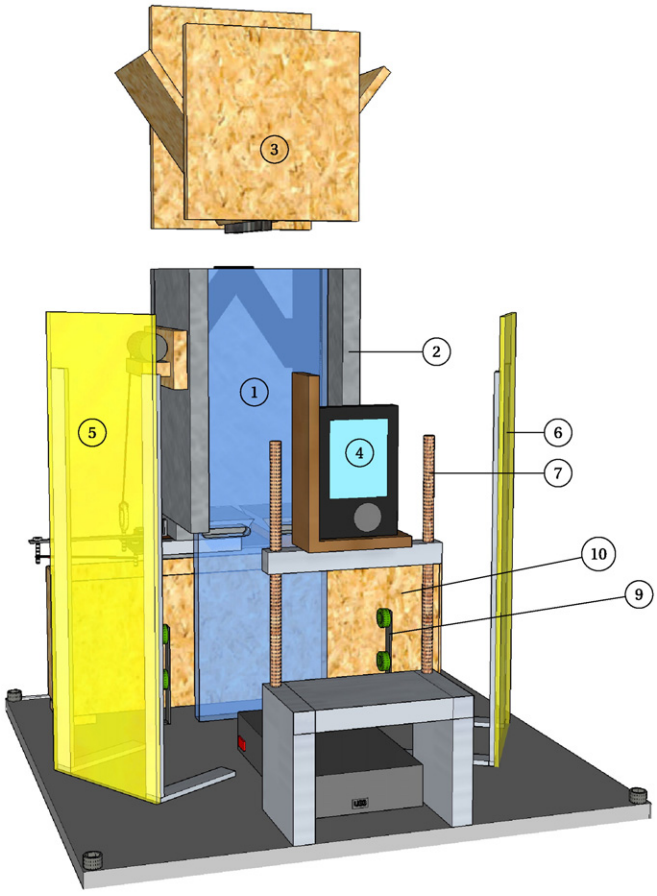

Fig. 3. Sketch of model silo outside of centrifuge. 1—acrylic window, 2—side wall, 3—filling funnel, 4—camera, 5 and 6—LED array, 7—camera stand, 9—vertical roller, and 10—collection bucket.

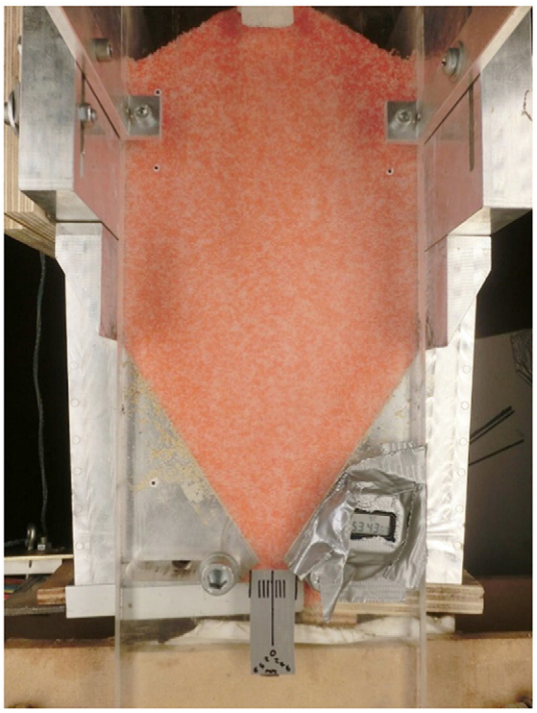

Fig. 4. Photograph of model silo showing stopwatch and grid points.

The location of the outlet 210 mm above the model base plate was chosen as the lowest possible height where the silo could be expected to discharge completely for the range of granular materials likely to be tested. This is only defined approximately because different materials have different angles of repose and the angle of repose was observed during tests to decrease with increasing gravity[1]. The height of the top of the silo was simply the maximum possible that would fit in the centrifuge.

The interior of the model silo is completely smooth, there are no screw holes or protrusions in the walls. The only interruptions to planar aluminium or acrylic walls are the flush joints of neighbouring metal pieces positioned next to each other. The discharge rate is measured by load cells beneath the collection bucket. Flow behind the front acrylic wall is observed using a high-speed video camera and lighting set-up. The silo is opened by remotely releasing a spring loaded sliding door. The high-speed video camera is operated manually and is started before the centrifuge test begins. A view of the silo before discharge from the high-speed camera is shown in Fig. 4.

4. Instrumentation

4.1. High-speed video

High-speed video captures material movement at 232 FPS with a resolution of 512×384 pixels. Particle image velocimetry and image analysis techniques are applied to the video frames to investigate flow. The frame rate was verified by placing a stopwatch in the frame and measuring the time interval between sets of frames.

4.2. Particle image velocimetry

Particle image velocimetry is a technique for measuring the movement of solids or fluids. In this research, the open-source PIV software

[1] This influence of gravity on angle of repose has also been observed by Kleinhans et al. [12].

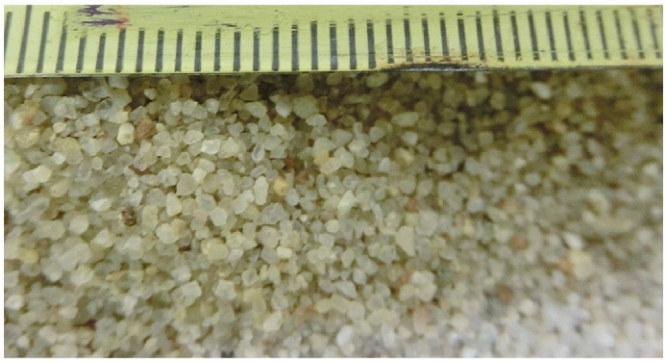

Fig. 5. Photograph of material M1, fine sand.

PIVLab (v.1.32) was used to interpret frames from the high-speed video. The technique to calculate displacement vectors between pairs of frame is as follows: Each image is divided into a large number of square regions, each covering only a small number of grains. Each area should have a unique combination of grey-scale pixel values (texture), this can make PIV unsuitable for use with materials which display little texture (unless markers may be used). In order to increase the texture in each region, the contrast is increased using Contrast Limited Adaptive Histogram Equalisation (CLAHE). Sets of displacement vectors between pairs of frames are calculated using the cross correlation through Fast Fourier Transform (FFT) technique with linear window deformation interpolator.

In images with low texture it is possible for vector magnitude to be underreported, as well as for false (wild) vectors to be computed. Wild vectors have dissimilar magnitude to their neighbours and can be removed using statistical techniques to identify outliers. In this research, a conservative vector validation technique is used where only vectors that vary more than 7 standard deviations from the average are replaced with vectors interpolated from neighbouring vectors. Small displacement vectors may be calculated due to low contrast in the images creating regions which lack unique texture and leads to false identification of the regions location in the second frame. As the software searches for the location of the region in the second frame, it begins at the original location of the test region and tests candidate regions off-set from this original location by an increasing amount. If regions are not adequately unique then a statistically significant match will be found prematurely and the displacement under-reported. In this research, the impact of these errors is reduced by temporal averaging of the displacement vectors between 10% and 40% of silo discharge, when the flow profile is stable.

The length unit of the vectors is converted from pixels to metres by specifying two points in the image which are a known distance from each other. By specifying the separation of the points in metres a conversion from pixels to metres is possible. The time between frames is calculated outside of PIVLab and is manually input. The frame rate of the video was verified by using a stopwatch in the video frame.

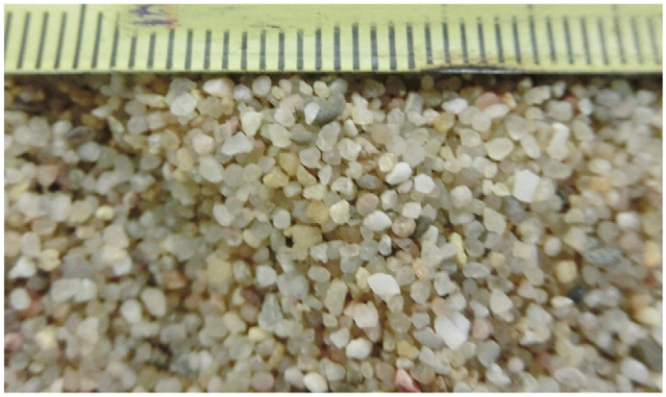

Fig. 6. Photograph of material M2, coarse sand.

Fig. 7. Photograph of material M3, glass beads mixture.

4.3. Load cells

Load cells beneath the collection bucket record the load from the bucket and its contents. This is used to calculate the mass discharge rate from the silo during discharge. Two miniature load cells are used, each with a rated capacity of 1 kN. The collection bucket is kept in place by guide rails designed to apply only horizontal forces to the collection bucket and this ensures that all vertical load is transmitted through the load cells.

5. Granular materials

Three materials are used during the tests, as detailed in Tables 2–4. A poorly graded fine sand (DIN EN 12904), a poorly graded coarse sand (DIN 1164/58) and a bi-disperse mixture of glass beads. These are labelled M1–M3 respectively. Material properties are shown in Tables 3 and 4.

Material M1 is fine sand "DIN EN 12904". It is used because its particle size distribution is poorly graded, it has well-defined properties and is readily available. Its bulk material properties are listed in Table 3.

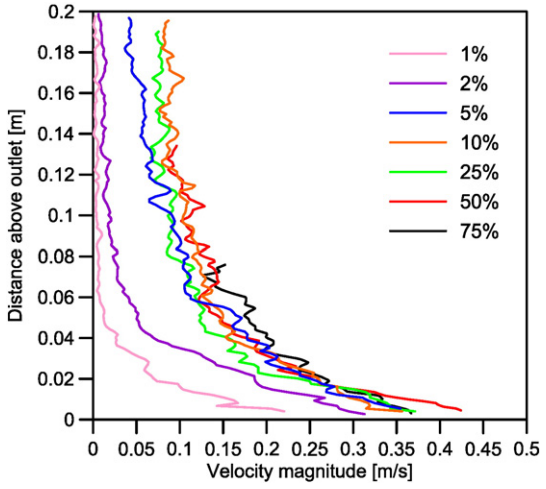

Fig. 8. Velocity magnitude of material above the outlet at different stages of discharge in silo with flat bottom.

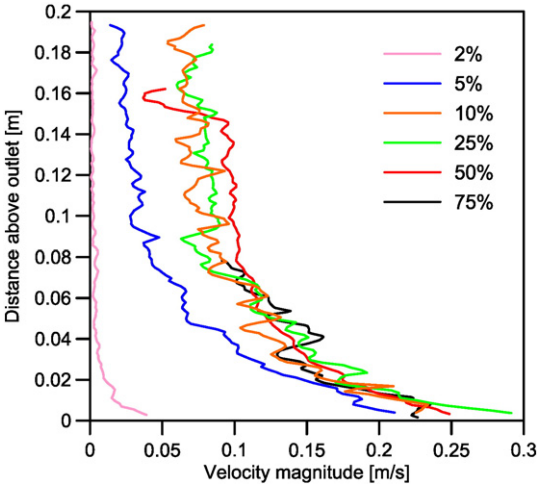

Fig. 9. Velocity magnitude of material above the outlet at different stages of discharge in silo with 30° hopper.

Material M2 is "DIN 1164/58 Norm Sand II" and is a coarse silica sand. It is poorly graded and has well-defined properties (Table 3).

Material M3 is industrially produced and has well defined material properties and limits of variability, which are detailed in Table 4.

6. Test procedure

Material is poured into the model silo at 1 *g* through a funnel designed for use with the model silo. The mass of material in the silo is calculated by measuring the mass of the storage bucket and funnel before and after filling. After the silo is filled, the high speed camera and lighting system is turned on and set. The silo-centrifuge model is then accelerated and held at an angular velocity corresponding to 5 *g*, 10 *g* or 15 *g* at the silo outlet. Tests at 1 *g* were made whilst the centrifuge was stationary.

Silo discharge is initiated by activating a servo-motor. This causes a spindle attached to the motor to pull a pin which releases a spring-loaded sliding silo door which moves away from the silo outlet leaving it unobstructed. The load cells record the force exerted by the collection bucket and its contents.

Once discharge is complete, the centrifuge is decelerated until the beam is stationary. The load cell data then stops being recorded and

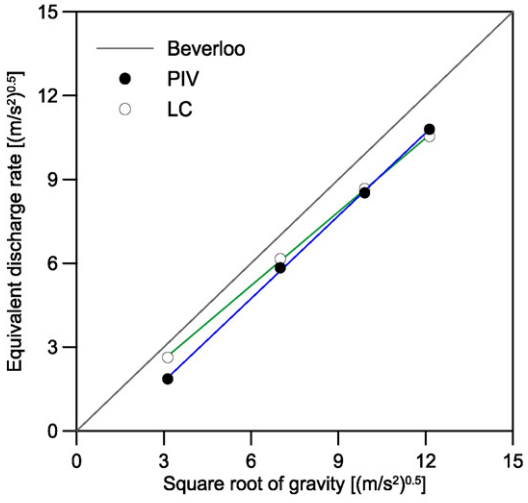

(a) Silo with flat bottom

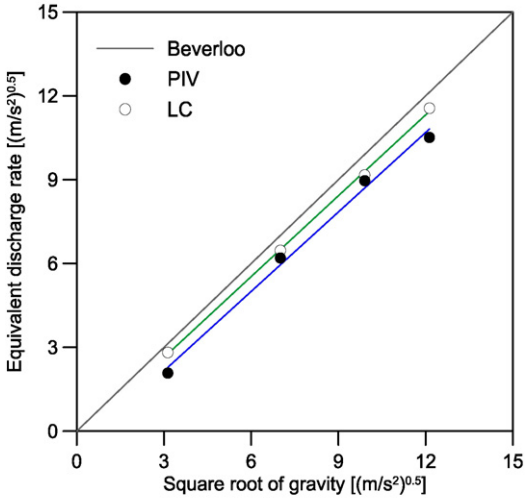

(b) Silo with 30 degree hopper

Fig. 10. Equivalent discharge rates, material M1 — fine sand.

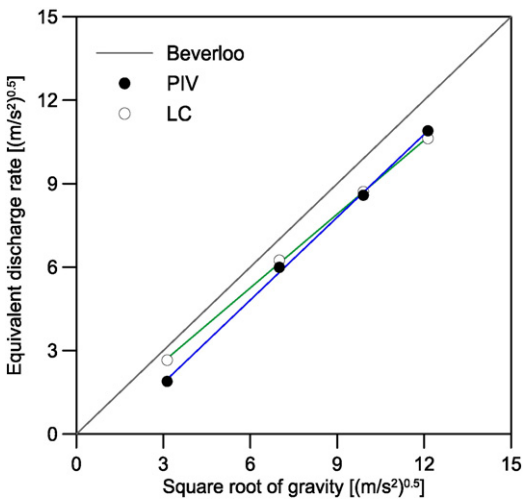

(a) Silo with flat bottom

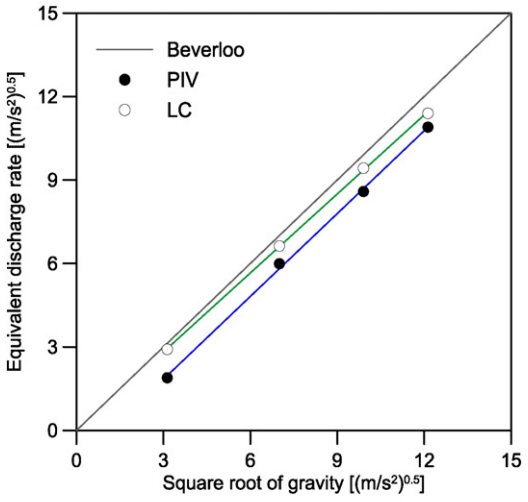

(b) Silo with 30 degree hopper

Fig. 11. Equivalent discharge rates, material M2 — coarse sand.

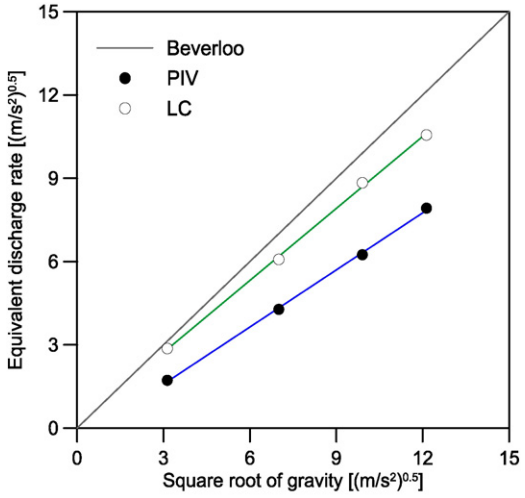

(a) Silo with flat bottom

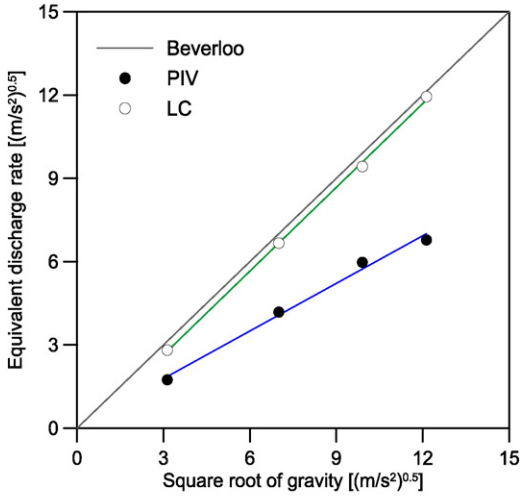

(b) Silo with 30 degree hopper

Fig. 12. Equivalent discharge rates, material M3 — glass beads.

the centrifuge is turned off. The centrifuge is then opened and the high-speed video camera and lights are also switched off.

Tests at a specific acceleration are repeated until 3 tests with less than 5% variation in discharge rate are obtained. Values used to calculate expected discharge rate using the Beverloo correlation are shown in Table 5.

7. Results

7.1. Method of analysis

Key features of the procedure used to produce the results include adjusting the load cell data to account for the location of the centre of mass of the discharged material relative to the axis of rotation, and assumptions underlying the PIV analysis including spatial and temporal averaging of the patch vectors.

The readings from the load cells are adjusted to consider the increased radius of the centre of mass of the discharged material and are used to calculate the mass flow rate.

The high-speed camera records the movement of grains behind the transparent acrylic wall. Only the front layer of particles is visible to the camera and therefore only the front layer of particles are considered in the PIV analysis. A velocity profile is calculated across the width of the silo using data output from the particle image velocimetry (PIV) analysis. Considering the principles of conservation of mass and planar flow, the discharge rate is calculated using this PIV data as well as from the load cell's data. These two methods are independent of each other and the similarity between the two techniques is used to assess the accuracy of the PIV results.

The discharge rate is calculated via PIV by integrating the flow profile across the width of the silo and assuming planar flow. This gives only an approximation of the mass flow rate because some friction with the walls will inevitably produce shear gradients. However for materials M1 and M2, the flow rates calculated according to these two methods are nearly identical and therefore the friction force between the front or back wall and the granular material seems to have little effect on the flow rate. Full validation of the approximations and techniques employed, including flow acceleration and free-flowing discharge are found in Mathews [13].

The acceleration of material in a region of the silo directly above the outlet was investigated in order to quantify the length of time it took for

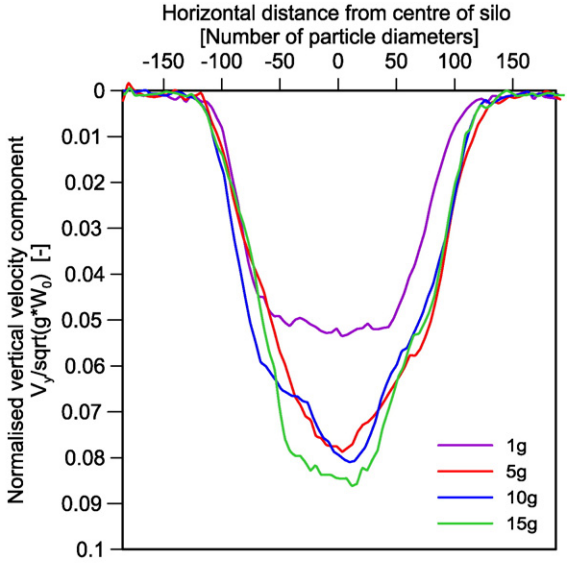

(a) Vertical component

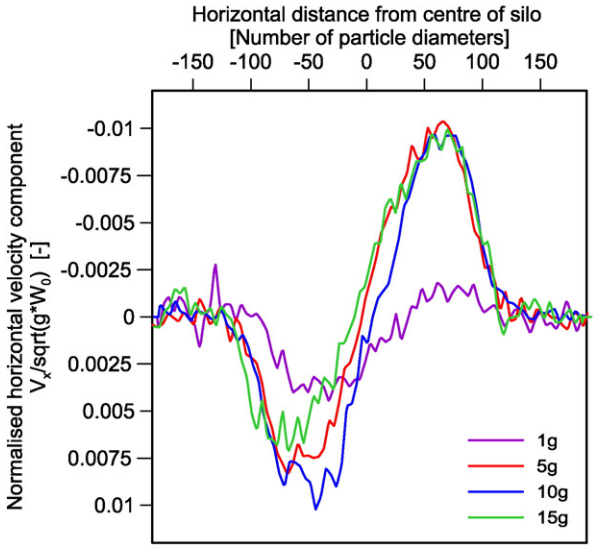

(b) Horizontal component

Fig. 13. Normalised components of flow profiles, material M1 — fine sand, silo with flat bottom.

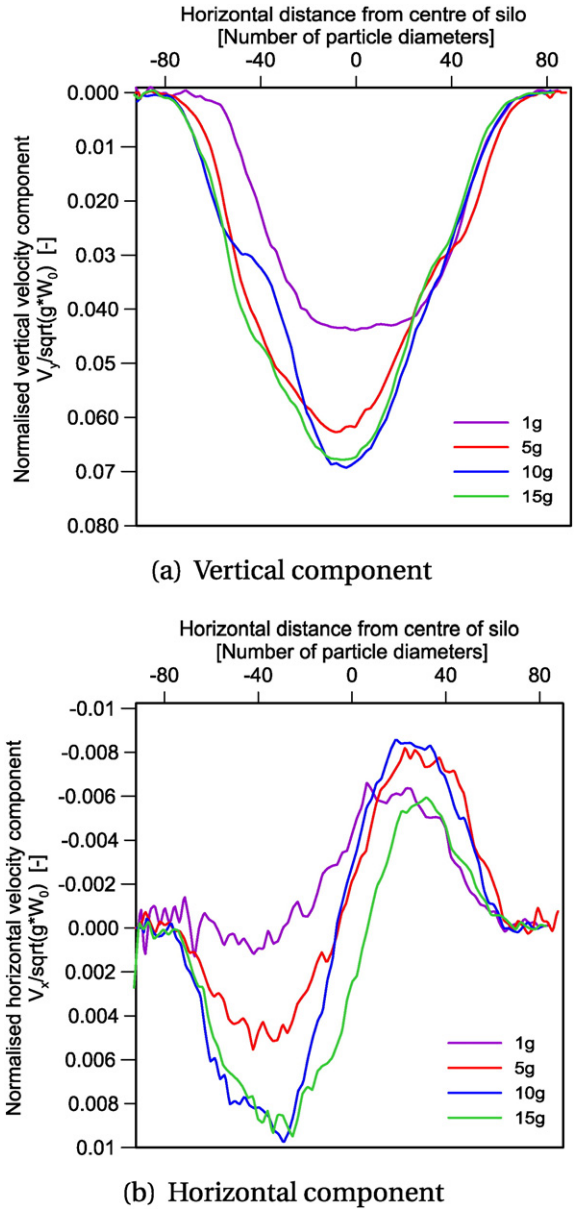

Fig. 14. Normalised components of flow profiles, M2 — coarse sand, silo with flat bottom.

the flow pattern to become stable in the bottom half of the silo. Once it is known when the flow pattern becomes stable, a time-averaging method can be reliably used. Figs. 8 and 9 show that once the silo is 5% discharged (in the case of the flat bottomed silo) or 10% discharged (in the case of the silo with a hopper) the flow pattern is stable.

This time-averaging method is used to find the temporally-averaged flow profile of material inside the silo along a horizontal line 112 mm above the silo outlet. This is the average flow profile between 10% of silo discharge and 40% of silo discharge.

7.2. Equivalent discharge rates

The observed discharge rates are compared to either the Beverloo model for flat-bottomed silos, or to an adjusted Beverloo model for the silo with 30° hopper. The value of the C coefficient is 1.03 and the value of the k coefficient is 1. Inspection of the Beverloo correlation shows that the discharge rate is predicted to be proportional to the square root of the acceleration due to gravity.

Figs. 10 to 12 present an "Equivalent Discharge Rate" defined as the discharge rate divided by the non-gravitational terms of the Beverloo correlation (Eq. (12)). This is plotted against the square root of the gravity ($\sqrt{g}$). A linear regression trendline has been applied and the coefficient of determination, gradient and intercept of the regression for each condition are shown in Tables 6 and 7. From Eq. (12) it is clear that if the discharge rate is described by the Beverloo correlation, then the equivalent discharge rate plotted against the square root of the gravity will have gradient 1 and intercept 0.

The high coefficients of determination show that discharge rate is linearly proportional to the square rate of the gravity but the gradient of the linear regression trend line is consistently smaller than 1. Across all materials using discharge rates calculated from the load cell data, the average gradient is 0.8760 for the flat bottomed silo, implying that $Q \propto 0.7674\sqrt{g^*}$, and 0.9720 for the silo with 30° hopper, implying that $Q \propto 0.9448\sqrt{g^*}$. This shows that discharge rates are more sensitive to gravity in silos with hoppers than in flat bottomed silos. Possible mechanisms to explain this include the role of locking or jamming mechanisms between the grains of the ensiled material, which are governed by gravitational forces. It is interesting to note that material

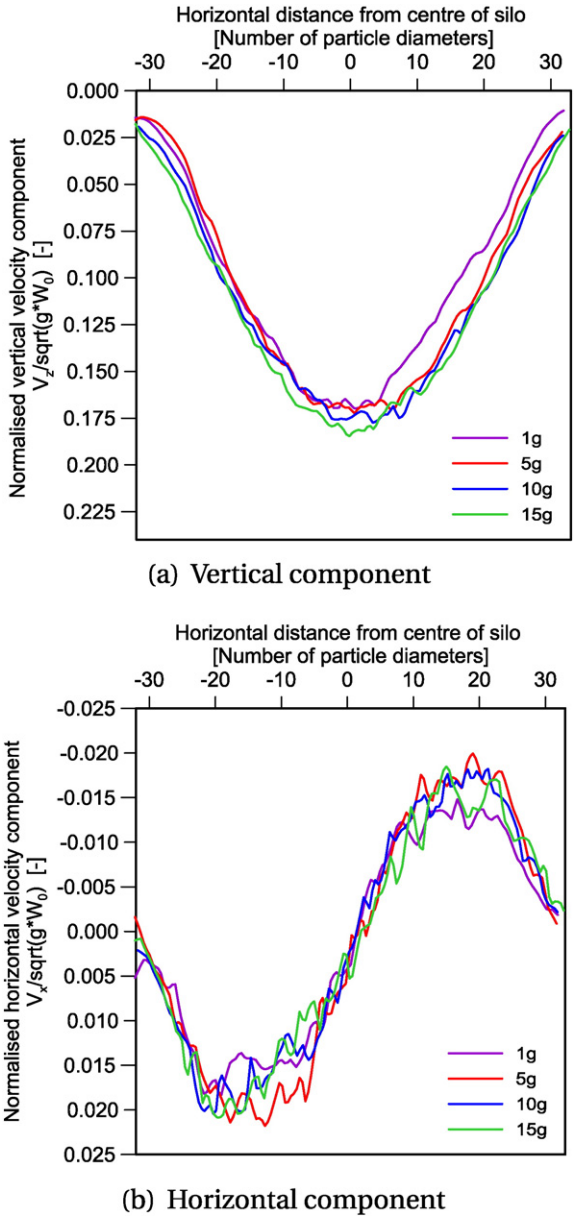

Fig. 15. Normalised components of flow profiles, material M3 — glass beads, silo with flat bottom.

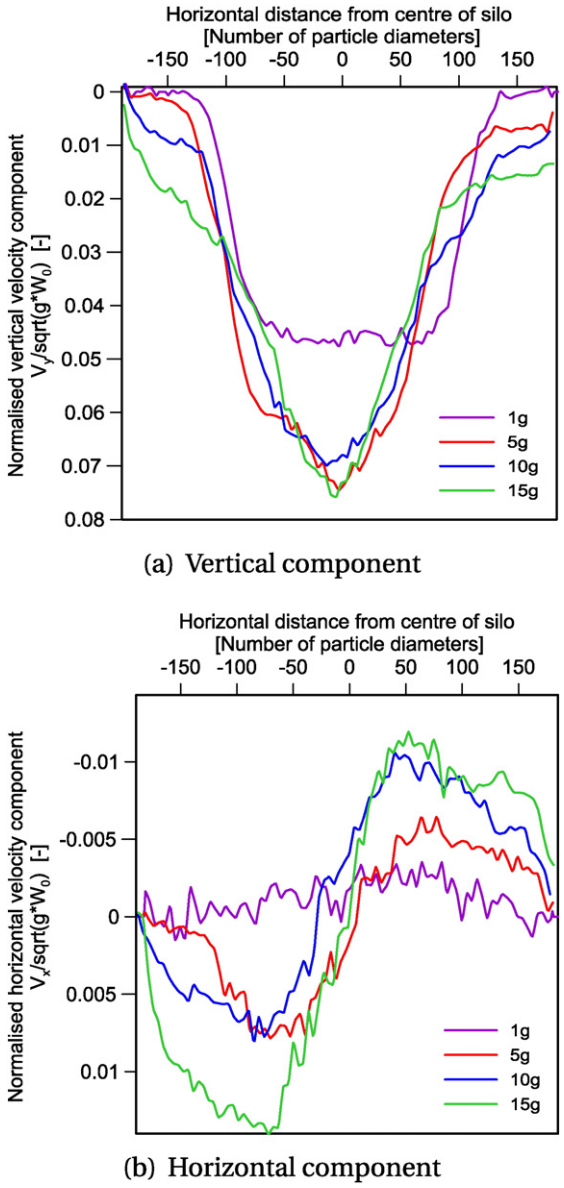

Fig. 16. Normalised components of flow profiles, M1 — fine sand, silo with 30° hopper.

M3, which is spherical and has a low friction angle, produces results very close to those expected by the Beverloo correlation for the case of the silo with hopper. However in the case of the flat bottomed silo, M3 produces the results least consistent with the Beverloo correlation.

The intercept of the equivalent discharge rate is generally less than 0 (Tables 6 and 7). This implies that a minimum gravitational acceleration is required before the silo will discharge. This may be due to the resistance to flow generated by the irregular shaped particles. If the theoretical gradient of 1 is achieved, this threshold gravitational acceleration is c^2 m s^{-2}.

$$W_{equivalent} = W_{observed}/(W_{Bev}/\sqrt{g}) = W_{observed}/(C\rho_b(l-kd)(W_0-kd)^{1.5}) \quad (12)$$

The discharge rate predicted by the Beverloo correlation is approximately 10% larger than those observed for materials M1 and M2. For the coarse and fine sands (Figs. 10–11), the particle image velocimetry analysis shows good results at gravities greater than 1, which can lead to quantitative analysis of flow profiles within the silo. Fig. 12 shows that the PIV results significantly under-report the discharge rates for glass beads. This shows the importance of material texture for PIV analysis. Therefore for tests with glass beads only a qualitative discussion of the results is possible. The PIV analysis also under-reports the discharge rates of materials M1 and M2 at $N=1$.

7.3. Normalised flow profiles

The normalised flow profiles in Figs. 13–18 compare the internal flow behaviours of the silo during discharge at different gravities. The normalisation technique is shown in Eq. (13) where $V_{i,n}$ is the normalised velocity in direction i at gravity factor n ($n=g^*/g$), V_i is velocity in direction i, W_0 is the width of the silo outlet and g^* is the magnitude of the acceleration. The normalised profiles are calculated along a horizontal line 112 mm above the silo outlet. In the silo with 30° hopper, this corresponds to the transition between the hopper and vertical sections.

$$V_{i,n} = \frac{V_i}{\sqrt{g^* W_0}} \quad (13)$$

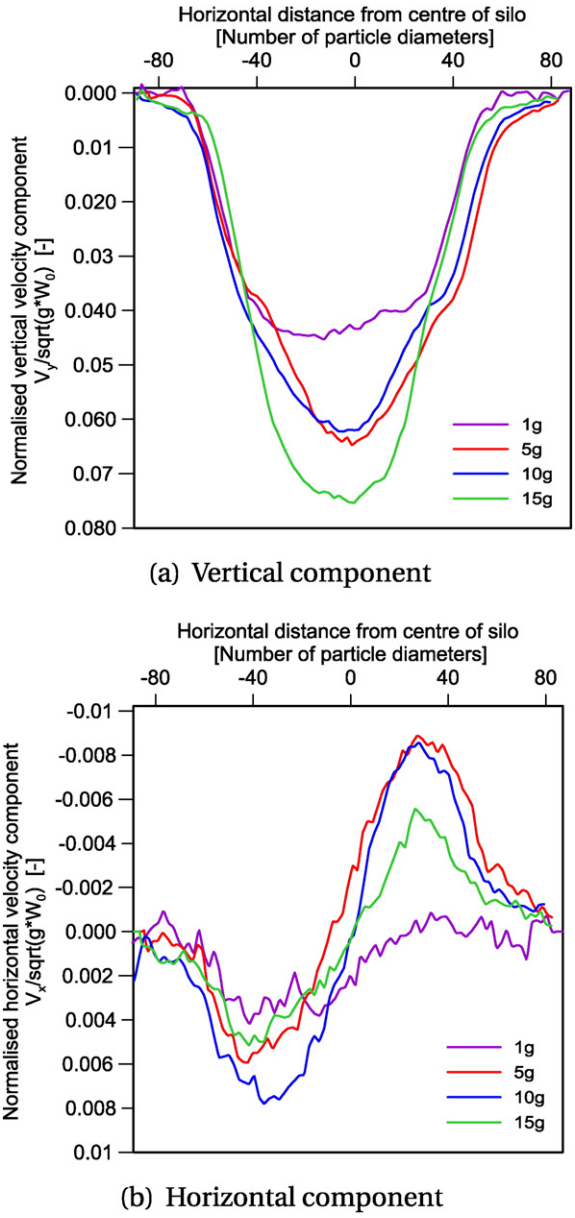

Fig. 17. Normalised components of flow profiles, material M2 — coarse sand, silo with hopper.

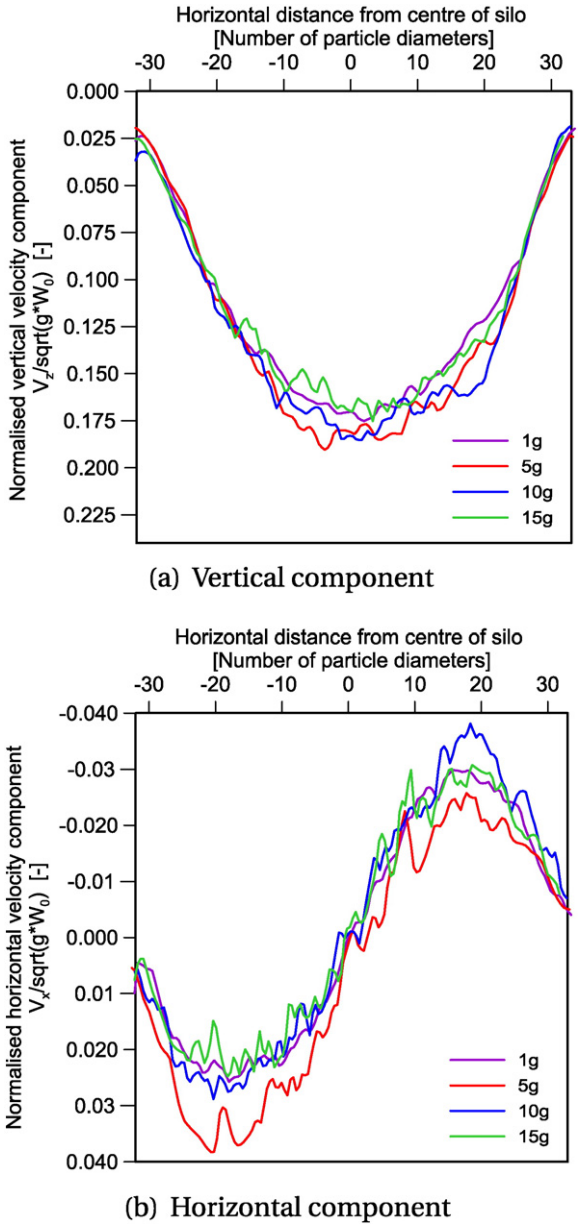

Fig. 18. Normalised components of flow profiles, material M3 — glass beads, silo with hopper.

Material M1 discharges with a flow pattern at 1 *g* that is significantly different to its flow pattern at higher gravities. This is seen from the decreased peak of the normalised velocity profile in Figs. 13a and 16a. At gravities 5 *g*, 10 *g* and 15 *g* the normalised flow profiles have a high degree of similarity, but contrast with the flow profiles at 1 *g*.

In Fig. 16a material M1 shows a behaviour in the hopper that is not observed with the other materials. The velocity of material sliding against the wall of the silo increases with increasing gravity. It is also seen that the flow pattern is only proportional to $\sqrt{g^* W_0}$ towards the centre of the silo between approximately ±75 particle diameters. At widths greater than this, the vertical component of the flow velocity increases at a rate greater than $\sqrt{g^* W_0}$. However, significant asymmetry is observed and the causes and consequences of this are discussed below.

Figs. 13b and 16b show the horizontal component of material M1's flow velocity along the same horizontal line 112 mm above the outlet. The trends are compatible with the observations drawn from the vertical component plots in Figs. 13a and 16a. It is seen that the normalised horizontal velocity components at 1 *g* are significantly smaller than at gravities higher than 1 *g*. In Fig. 16b there is a higher degree of asymmetry which corresponds to the asymmetry observed in Fig. 16a. The collapsing of velocity profiles onto approximately the same normalised profile at all factors of gravity greater than 1, for both velocity components, suggests that the flow field in a silo is independent of the gravitational acceleration.

Fig. 17a shows that for material M2, no slip is observed along the silo walls at any gravity, i.e. mass flow is never observed, unlike with the fine sand (M1). This is unexpected because the two materials have similar properties including angle of internal friction ($\theta_i \approx 35^\circ$) and bulk density.

Material M2 also shows a different behaviour at 1 *g* than at other gravities (Figs. 14a and 17a). This is similar to observations of material M1 (Figs. 13a and 16a). The normalised vertical component of the flow profile at 1 *g* is significantly smaller than it is at 5 *g*, 10 *g* or 15 *g* (Figs. 14a and 17a). Fig. 14a shows that in the silo with a flat bottom, the peak-normalised vertical flow at the centre of the silo is approximately 35% smaller than it is at 5 *g*, 10 *g* or 15 *g*. In the silo with 30° hopper (Fig. 17a), the peak-normalised velocity component is 30% smaller than the average normalised velocity component at other gravities, though there is a larger variation in the results at 5 *g*, 10 *g*, and 15 *g*.

Figs. 14b and 17b show the horizontal component of velocity and show that the degree of symmetry is less than that observed in material M1.

Figs. 15b–18b show that material M3 "Bi-disperse mixture of spherical glass beads" produces a very smooth set of normalised flow profiles. Mass flow is observed in all cases, as is evidenced by the non-zero normalised velocity components at the edges of the silo. The difference between the peak normalised velocity components at different gravities is also small.

Material M3 has a very low angle of internal friction ($\approx 22^\circ$), therefore it is expected that mass flow would be observed as well as a wide and shallow flow profile. The highest degree of symmetry is also expected in the smoothest material with the least internal shear, this is

Table 2
List of materials.

Material	Label	Properties	Photograph
Fine sand	M1	Table 3	Fig. 5
Coarse sand	M2	Table 3	Fig. 6
Glass beads	M3	Table 4	Fig. 7

Table 3
Properties of materials M1, fine sand DIN EN 12904 and M2, coarse sand DIN 1164/58 Normsand II.

Property	M1	M2
Material density ρ_s [g/cm^3]	2.650	2.644
Density range ρ_{min},ρ_{max} [g/cm^3]	1.40–1.60	1.44–1.65
Average particle diameter D_{50} [mm]	0.4	0.85
Void ratio $e_{min}e_{max}$ [–]	0.656–0.893	0.607–0.844
Coefficient of uniformity U [–]	1.5	1.4
Friction angle θ_i [°]	35	35

Table 4
Properties of material M3, bi-disperse mixture of glass beads.

Property	M3
Material density ρ_s [g/cm^3]	2.750
Bulk density ρ_b [g/cm^3]	1.52
Particle diameters d_1,d_2 [mm]	3.15 ± 0.1, 1.45 ± 0.1
Void ratio e [–]	0.809
Coefficient of uniformity U [–]	2.17
Friction angle θ_i [°]	22

Table 5
Values used for flow rate prediction.

Property	Fine sand (M1)	Coarse sand (M2)	Glass beads (M3)
Bulk density ρ_b [kg/m^3]	1500	1545	1520
Mean particle diameter d_0 [m]	4E−4	8.5E−4	2.3E−3
C [–]	1.03	1.03	1.03
k [–]	1	1	1
Outlet diameter W_0 [m]	0.01	0.01	0.03

observed. Figs. 15b and 18b show that horizontal component of material flow is also highly symmetric.

8. Conclusion

The effects of gravity on a discharging silo centrifuge model have been investigated using three materials at gravities between 1 *g* and 15 *g* using high-speed video, particle image velocimetry and load cells.

Tests were conducted in a silo centrifuge model developed for use in the geotechnical centrifuge at the BOKU, Vienna. The model set-up is symmetric about the vertical axis. The granular response to gravity was investigated by measuring the mass discharge rate and internal flow velocities.

8.1. Silo discharge rates at increased gravities

Silo discharge rate is shown to be proportional to the square root of the gravity. The mass discharge rate is quantified using two independent instrumentation types. Load cells beneath the collection bucket give one measure of discharge rate while calculations based on PIV analysis give another independent measure. The two methods show the same trend when frames from high-speed video of the granular material have adequate texture. Materials with adequate texture for the PIV analysis are M1 and M2. Material M3 gives mediocre quality results.

The observed discharge rate is compared to the discharge rate predicted using the Beverloo correlation. The Beverloo correlation was calculated using a k value of 1 throughout the analysis and this led to a consistent over-prediction at all gravities, although the magnitude varied between materials. A value of $k = 1.6$ gives the smallest error across all materials, however a value of 1 was used throughout this investigation due to the lack of an analytical reason to justify a value greater than 1.

For materials M1 and M2 (poorly graded sands) discharging from the flat bottomed silo, the Beverloo discharge rate is a more accurate predictor of discharge rate at lower gravities, before mechanisms not considered by the Beverloo correlation become increasingly effective at impeding flow at higher gravities. In the silo with 30° hopper, the difference between observed and predicted discharge rates is not proportional to the gravity.

The predicted discharge rates for material M3 (glass beads) discharging from the silo with 30° hopper were very close to those observed using load cells. For the flat-bottomed silo the difference between observed and predicted discharge rate was greater than for any other material.

Table 6
Equivalent discharge rates derived from load cell data: Linear trend analysis.

Material	Gradient	Intercept	Coeff. of determination
Silo with flat bottom			
M1	0.8796	−0.0773	0.9997
M2	0.8840	−0.0512	0.9995
M3	0.8645	0.1318	0.9989
Silo with hopper			
M1	0.9645	−0.2547	0.9992
M2	0.9462	−0.0184	0.9997
M3	1.0054	−0.3748	0.9991

Table 7
Equivalent discharge rates derived from PIV data: Linear trend analysis.

Material	Gradient	Intercept	Coeff. of determination
Silo with flat bottom			
M1	0.9870	−1.1855	0.9996
M2	0.9923	−1.1385	0.9989
M3	0.6856	−0.4724	0.9992
Silo with hopper			
M1	0.9478	−0.6851	0.9936
M2	0.9923	−1.1385	0.9989
M3	0.5717	0.0709	0.9909

The PIV technique consistently undervalues the discharge rate at 1 *g* for all three materials, leading to large differences in the discharge rates calculated by the load cells and the PIV technique. The difference between the two techniques reduces at higher gravities and it is suggested that this is due to the effects of friction between the ensiled material and the front silo wall being more significant at 1 *g* than at higher gravities. For material M3 the difference between the two discharge calculation techniques increases with gravity, this is probably a consequence of an inadequate frame rate in the high speed video footage from which the PIV data is derived.

8.2. Flow profiles during discharge at increased gravities

Determination of the factors controlling funnel flow or mass flow conditions would benefit granular materials engineering. It is shown that the location of the flow intersection with the wall is independent of gravity and therefore the flow pattern is independent of gravity.

The velocity of the granular material during discharge was investigated in the following ways:

1. The vertical component of flow was quantified at 4 different gravities: The flow is recorded using high-speed video and analysed using PIV. When the vertical component of the flow is considered it is seen that normalising the velocity distribution according to $V_{z,n} = V_z/\sqrt{g^* W_o}$ produces flow profiles that take approximately the same shape and magnitude. This shows that V_z is proportional to $\sqrt{g^*}$.
2. The horizontal component of the flow was considered at the same gravities and the same normalisation method was applied $V_{x,n} = V_x/\sqrt{g^* W_0}$.

Considering the horizontal component of the flow, the same relationship with gravity is seen where V_x is proportional to $\sqrt{g^*}$. Intriguing sine waves are produced with 0 amplitude at the walls and silo centre line and the same normalised amplitude.

For both horizontal and vertical velocity components, the velocity profile is often asymmetric about the silos vertical axis. Given the vertically symmetric model set-up and the vertically symmetric filling procedure, the source of this asymmetry is not obvious. The degree of asymmetry is not consistent between either materials or gravitational acceleration, and further investigation of the mechanisms producing it is desirable.

The normalised vertical and horizontal velocity profiles approximately collapse for all gravities except at 1 *g*, except in the case of material M3. This correlates with the under-reported mass discharge rates calculated using PIV at 1 *g*. For material M3 the difference between the mass discharge rate calculated using the PIV technique and the load cells is constant across all gravities. This consistency explains why for material M3 all the normalised velocity profiles collapse to form the same approximate shape, but this is not observed for materials M1 and M2 where the normalised velocity profile for 1 *g* does not lie with the other normalised velocity profiles.

Acknowledgements

This research was undertaken as part of the PARDEM Initial Training Network. It was funded by the Marie Curie Actions and the European Union's Research Framework 7 (238577) programme. The financial support for this project is gratefully acknowledged.

References

[1] W.A. Beverloo, H.A. Leniger, J. van de Velde, The flow of granular solids through orifices, Chem. Eng. Sci. (1961) 260–269.
[2] Y.C. Chung, J. Ooi, A study of influence of gravity on bulk behaviour of particulate solid, Particuology 6 (2008) 467–474.
[3] S. Dorbolo, L. Maquet, M. Brandenbourger, F. Ludewig, G. Lumay, H. Caps, N. Vandewalle, S. Rondia, M. Melard, J. van Loon, A. Dowson, S. Vincent-Bonnieu, Influence of the gravity on the discharge of a silo, Granul. Matter 15 (2013) 263–273.
[4] D.J. Ewalt, F.H. Buelow, The flow of granular solids through orifices, Q. Bull. Mich. Agric. Exp. Stn. 46 (1) (1963) 92–102.
[5] Ferstl, Modellversuche zum ErddruckPh.D. thesis Universitaet fuer Bodenkultur, Vienna, 1998.
[6] R.T. Fowler, J.R. Glastonbury, The flow of granular solids through orifices, Chem. Eng. Sci. 10 (1959) 150–156.
[7] M. Goldschmidt, J. Link, S. Mellema, J. Kuipers, Digital image analysis measurements of bed expansion and segregation dynamics in dense gas-fluidized beds, Powder Technol. (2003) 135–159.
[8] C. Gutberlet, R. Katzenbach, K. Hutter, Experimental investigation into the influence of stratificationon on the passive earth pressure, Acta Geotech. 8 (2013) 497–507.
[9] H. Janssen, Versuche ueber getreidedruck in silozellen, Z. Ver. Dtsch. Ing. (1895) 1045–1049.
[10] A.W. Jenike, Storage and flow of solids, University of Utah, Salt Lake City, 1964.
[11] M. Ketchum, Design of walls, bins and grain elevators, McGraw-Hill, New York, 1907.
[12] M.G. Kleinhans, H. Markies, S.J. de Vet, A.C. in't Veld, F.N. Postema, Static and dynamic angles of repose in loose granular materials under reduced gravity, J. Geophys. Res. Planets 116 (2011) E11004, http://dx.doi.org/10.1029/2011JE003865.
[13] J. Mathews, Investigation of granular flow using silo centrifuge modelsPh.D. thesis Universitaet fuer Bodenkultur, Vienna, 2013.
[14] M.E. Myers, M. Sellers, Final-year project reportMaster's thesis Department of Chemical Engineering, Cambridge, 1977.
[15] R.M. Nedderman, Statics and kinematics of granular flow, Cambridge University Press, Cambridge, England, 1992.
[16] M. Ostendorf, J. Schwedes, Application of particle image velocimetry for velocity measurements during silo discharge, Powder Technol. 158 (2005) 69–75.
[17] H.F. Rose, T. Tanaka, The engineer (London), 1956 208.
[18] S.M. Rubio-Largo, A. Janda, D. Maza, I. Zuriguel, R.C. Hidalgo, Disentangling the free-fall arch paradox in silo discharge, Phys. Rev. Lett. 114 (2015) 238002, http://dx.doi.org/10.1103/PhysRevLett.114.238002 (URL: http://link.aps.org/doi/10.1103/PhysRevLett.114.238002).
[19] A.N. Schofield, Cambridge geotechnical centrifuge operations, Geotechnique 30 (1980) 227–268.
[20] D. White, W. Take, M. Bolton, Soil deformation measurement using particle image velocimetry (PIV) and photogrammetry, Geotechnique 53 (2003) 619–631.
[21] L. Zhuang, Y. Nakata, U. Kim, D. Kim, Influence of relative density, particle shape, and stress path on the plane strain compression behavior of granular materials, Acta Geotech. 9 (2014) 241–255.